UNCLASSIFIED

Defense Technical Information Center
Compilation Part Notice

ADP012202

TITLE: Insight into the Formation of Ultrafine Nanostructures in Bulk Amorphous Zr[54.5]Ti[7.5]Al[10]Cu[20]Ni[8]

DISTRIBUTION: Approved for public release, distribution unlimited

This paper is part of the following report:

TITLE: Nanophase and Nanocomposite Materials IV held in Boston, Massachusetts on November 26-29, 2001

To order the complete compilation report, use: ADA401575

The component part is provided here to allow users access to individually authored sections of proceedings, annals, symposia, etc. However, the component should be considered within the context of the overall compilation report and not as a stand-alone technical report.

The following component part numbers comprise the compilation report:
ADP012174 thru ADP012259

UNCLASSIFIED

Mat. Res. Soc. Symp. Proc. Vol. 703 © 2002 Materials Research Society V5.4

Insight into the Formation of Ultrafine Nanostructures in Bulk Amorphous $Zr_{54.5}Ti_{7.5}Al_{10}Cu_{20}Ni_8$

André Heinemann[2], Helmut Hermann[1], Albrecht Wiedenmann[2], Norbert Mattern[1], Uta Kühn[1], Hans-Dietrich Bauer[1], Jürgen Eckert[1]
[1]Institut für Festkörper- und Werkstofforschung Dresden,
PF 27 00 16, D-01171 Dresden, Germany
[2]Hahn-Meitner-Institut Berlin, Glienicker Straße 100,
D-14109 Berlin, Germany

Abstract

Bulk amorphous $Zr_{54.5}Ti_{7.5}Al_{10}Cu_{20}Ni_8$ is investigated by means of small-angle neutron scattering (SANS), differential-scanning calorimetry (DSC), high-resolution electron microscopy (HREM) and other methods. The formation of ultrafine nanostructures in the glassy phase is observed and explained by a new model. Structural fluctuations of randomly distributed partially ordered domains grow during annealing just below the glass transition temperature by local re-ordering. During annealing the DSC gives evidence for a increasing volume fraction of the locally ordered domains. At high volume fractions of impinging domains a percolation threshold on the interconnected domain boundaries occurs and enhanced diffusion becomes possible. At that stage SANS measurements lead to statistically significant scattering data. The SANS signals are analyzed in terms of a model taking into account spherical particles surrounded by diffusion zones and interparticle interference effects. The mean radius of the nanocrystalline particles is determined to 1 nm and the mean thickness of the depletion zone is 2 nm. The upper limit for the volume fraction after annealing at 653 K for 4 hours is about 20 %. Electron microscopy confirms the size and shows that the particle are crystalline.

Introduction

The mechanisms of nanostructure formation in amorphous precursors are of much current interest. According to the variability of chemical composition, short- and medium-range order, and preparation methods of metallic glasses [1], these materials show a great variety of physical and chemical properties. One of these properties is the ability of some amorphous alloys (e.g., Finemt, see [2]) of transforming into a nanostructured state during annealing. Both from the technological and physical point of view, it is important to understand the processes responsible for the transition from the homogeneous amorphous state into the nanostructured one. Several possible mechanisms of the formation of nanoscale structures in metallic glasses have been discussed: preformation of aggregates in the liquid state [3, 4, 5, 6], extremely high nucleation rate accompanied by decreased growth rate [7, 8], spinodal decomposition [9], decomposition within the amorphous state and subsequent crystallization of at least one of the amorphous phases [8, 10], homogeneous nucleation taking into account linked stochastic fluxes of interfacial attachment and diffusion in the cluster neighborhood [11], and a model considering inhibitors accumulating at the surface of the nanocrystals to be responsible for limited growth [12]. Recently, ultrafine nanostructures have been observed in Zr-based bulk

amorphous alloys. Crystal-like clusters [13] and nanocrystals [14] with mean grain size of 2 nm were detected and analyzed by means of X-ray diffraction(XRD) and HREM, respectively. It was shown [15, 16, 17] that partial crystallization of such alloys on a nanometer scale may have considerable influence on mechanical properties of the material. Here we

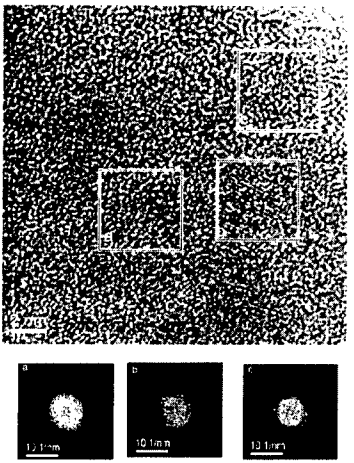

Figure 1: HREM image of the sample annealed for 240 min. at 653 K. For the marked areas a), b) and c) two dimensional fast fourier transformations were shown in separate pictures. In b) and c) a nanocrystal is visible.

examine the evolution of ultrafine nanostructures in bulk amorphous $Zr_{54.5}Ti_{7.5}Al_{10}Cu_{20}Ni_8$ during annealing in the glass transition range in order to find out the mechanisms of the structure formation.

Sample preparation and thermal treatment

The samples were prepared by a single roller melt spinning technique. By rapid quenching from the melt one obtains ribbons with a width of about 5 mm and a thickness of about 50 μm). The obtained as-prepared samples are homogeneous with respect to HREM and SANS. The SANS signal of the as-quenched state which contains only statistical noise was shown in figure 6. From this material a time-series of samples was prepared by annealing at 653 K for 15 min up to 240 min. The used temperature is slightly below the glass temperature T_g which is characterized by the estimates of the T_g(onset)= 660 K and T_g(inflection point)= 680 K temperatures of the glass transition region shown in figure 2. The thermal characterizations were made by using a Perkin-Elmer DSC 7 calorimeter at a heating rate of 40 K/min. The DSC plot for the as-prepared sample in a temperature range from 500 K to 850 K is shown in figure 2. Two exothermic events between 695 K and 740 K and above 740 K lead to an heat release of 19.7 J/g and 14.0 J/g, respectively. Annealing up to 873 K

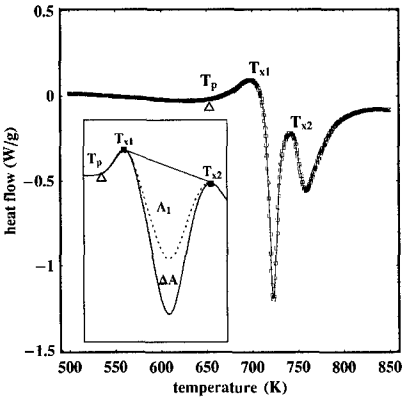

Figure 2: The heat flow measured with DSC technique. The DSC scan (40 K/min) shows two exothermic events. The total heat release between $T_{x1} = 695$ K and $T_{x2} = 740$ K is 19.7 J/g. For the second event ($T > 740$ K) one obtains 14.0 J/g. The annealing temperature of the samples was $T_p = 653$ K.

lead to a completely crystallized state with particles of about 50 μm in diameter. All the ultrafine nanostructures occur only below 740 K. The preparation temperature of 653 K was chosen because pre-experiments indicated that the time scale of transformation was good for our observations. The embedded picture in figure 2 outlines the procedure of the determination of the heat releases for the annealed samples. The difference (proportional to ΔA in the picture) between the heat release measured for the as-quenched sample (19.7 J/g) and the heat release obtained for the annealed one (proportional to A_1) was used to define the transformed volume fraction during this exothermic event in figure 5. The fractional heat releases for the sample series with different annealing times is used in figure 5 to describe the transformation kinetics.

Small-angle neutron scattering

The SANS experiments were carried out at the small-angle scattering facility V4 at the Berlin Neutron Scattering Center (BENSC). To characterize the global time evolution of the SANS signal on can calculate the scattering invariant I_2 defined (see e.g. [18]) by

$$I_2 = \int_0^\infty dq\, q^2 \left(\frac{d\sigma}{d\Omega}\right) \sim \sum_{i=1}^{N} \Delta q_i\, q_i^2 \left(\frac{d\sigma}{d\Omega}(q_i) - \left(\frac{d\sigma}{d\Omega}\right)_\infty\right) \quad . \tag{1}$$

The result of this analysis is shown in figure 3. The error bars arise from the experimental errors of $d\sigma/d\Omega(q_i)$ and the confidence interval of the background fit $(d\sigma/d\Omega)_\infty$. For two-phase systems I_2 is given by $c(1-c)\,\Delta\eta^2$ where $\Delta\eta$ is the scattering length density contrast

of the two phases and c the volume fraction of one of the phases. The behavior of I_2 versus annealing time differs in a fundamental manner from the DSC (see figure 5) and XDR results [13]. In the bound of the errors there is no change of the invariant during the annealing procedure up to 90 min. In contrast to the evolution of the heat release shown in figure 5. After 90 min. the heat release at this stage of the annealing process reaches over 70 %. This means the transformation process responsible for the observed heat release is not detectable in SANS. Then the value of I_2 changes significantly for 120 min, 180 min and 240 min annealing. This gives a hint to the presumption that a new kind of transformation process was actuated. This confirms to a significant change in the behavior of the heat release curve (see figure 5) and the viscosity curve (see figure 7) at that time.

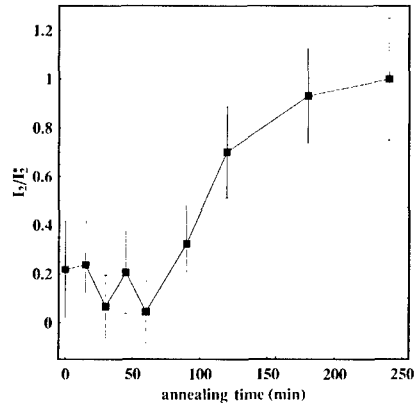

Figure 3: Evolution of the SANS scattering contrast versus annealing time. The scattering invariant I_2^* is equal to $(34 \pm 9) * 10^{-10}$ nm^{-4} sr^{-1}.

A qualitative analysis of the SANS data for the 120 min., 180 min. and 240 min. annealed samples is made with a model of polydisperse spherical particles with diffusion zones [19]. To take into account interparticle interferences we combine the Percus-Yevick approach according to [20] and our model in the following way:

$$I(q) = S(q, R_{hc}, c_p)|F(q, \mu, \sigma, l)|^2 \quad . \tag{2}$$

$|F(q, \mu, \sigma, l)|^2$ describes the contribution of the isolated gamma distributed spherical particles with diffusion zone where μ and σ are mean value and root mean square of the gamma distribution, respectively, and l characterizes the dimension of the diffusion zone (for details see [19]). $S(q, R_{hc}, c_p)$ is the contribution of the hard-core system with hard-core radius R_{hc} and volume fraction c_p and can be expressed in the Percus-Yevick approach as

$$S(q, R_{hc}, c_p) = \frac{c_p}{1 + c(2qR_{hc}, c_p)} \quad . \tag{3}$$

Table 1: Results of the least-square fit of the SANS data obtained from the 653 K / 240 min state. Mean values and limits of the 95% confidence intervals.

parameter	μ (nm)	σ (nm)	l (nm)	R_{hc} (nm)	c_p (%)
mean value	**0.96**	**0.34**	**2.2**	**5.2**	**17.2**
lower limit	0.85	0.31	1.6	3.7	7.0
upper limit	1.07	0.37	3.0	5.7	21.3

Here $c(x, c_p)$ is a function which can be calculated analytically (see e.g. [21, 22]). The experimental SANS data are fitted by equation (2) using a non-linear least-square routine. The results are given in table 1 and the quality of the fit was demonstrated in figure 6. The upper and lower bounds of the confidence intervals are not symmetric to the mean value. This is a consequence of the non-linearity of the fit. The confidence interval is chosen so that the true value of the parameter fitted can be found within this interval with a probability of 95%. The spatial distribution of the scattering length density for one particle with the Radius μ is shown in figure 4. It was shown [22] that for the samples annealed for

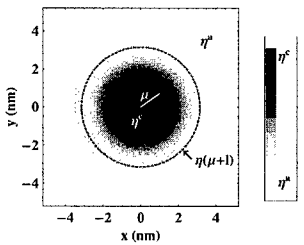

Figure 4: Radial profile of the scattering length density for a given particle.

120 min., 180 min. and 240 min. it is essential to use a model with diffusion zones to fit the data. The influence of the interparticle interferences together with a simple two-phase model (e.g. polydisperse spheres) cannot explain the SANS data. In our model this interferences permitted a estimate of the volume fraction of the particles. This estimate is crowing from about 7 % in the 120 min. case up to 17 % in the 240 min. case. The results of the particle sizes were confirmed by HREM in figure 1. The HREM images were taken with the 300 kV microscope TecnaiF30-STwin (FEI) at IFW Dresden after preparation in the Rapid Etching System RES010 (Bal-Tec) with flat striking Ar^+ ions. The embedded FFT pictures in figure 1 additionally shows that the particles are crystalline.

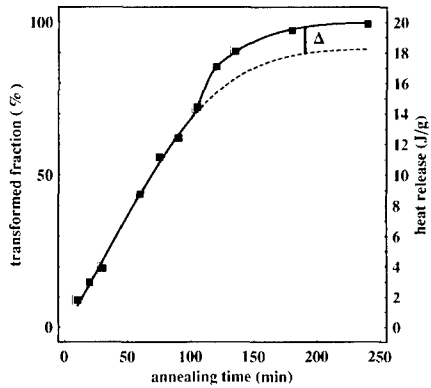

Figure 5: Time evolution of the fractional heat release during annealing. The solid line shows the theoretical curve $h_a(t) + h_b(t)$, the dashed line shows $h_a(t)$ for $t \geq h_b$.

Results and Discussion

The different behavior for the evolution of the SANS curves versus annealing time and the DSC curves guided to a model with two different processes during nanocrystallisation. The presented interpretation is based on the idea that the structure of a supercooled liquid alloy is heterogenous. Recent experimental (see e.g. [23, 24, 25]) and theoretical (see e.g. [26, 27, 28, 29]) workings discuss the influence of this assumption to physical properties. It might be expected that the reason for the type of nanostructuring described here is related to properties of the supercooled liquid state, especially to dynamical heterogeneities. We assume that in the supercooled liquid state different local configurations exists with different local free energy and correlation length. Annealing with a proper temperature enables cluster having a suitable free energy start to grow by rearranging of atoms or atom-groups at their surfaces. We state that the heat release in the DSC measurements up to about 100 min. rises from this process. If the growing clusters are distributed randomly in the material and all clusters participate in the growing process the well known Kolmogorov-Johnson-Mehl-Avrami (KJMA) model (see [30, 31, 32]) can be used to explain the growing of the clusters. If v_a is the transformed volume fraction the KJMA model predict a time evolution of this parameter to:

$$v_a = v_a^{max} \left(1 - \exp\left\{ A_0 (1 - (1 + \frac{v\,t}{r_0})^3) \right\} \right) \quad . \tag{1}$$

Here $1 - \exp\{-A_0\}$ is the volume fraction of the activated clusters at $t = 0$ and r_0 their mean radius at the beginning of growth. v describes the velocity of the cluster surface propagation during growing and in a first approximation v is supposed to be constant. In equation (1) it is supposed that the activated clusters have a finite size at the beginning of the growing process. If we assume, that the heat release h_a is proportional to the transformed volume

fraction v_a we can fit the DSC data with following equation.

$$h_a = h_a^{max}\left(1-\exp\left\{A_0(1-(1+\frac{v\,t}{r_0})^3)\right\}\right) \tag{5}$$

The result is shown in figure 5 as a dashed line.

For annealing times greater than approximately 100 min we learned from the SANS results, that a new process should occur to explain the increase of I_2 and the predicted particles with a mean radius of about 1 nm. The essential diffusion zone around the particles places us in the position to postulate the start of a diffusion controlled process after about 100 min. If we assume here again, that the heat release is proportional to the transformed volume fraction we can approximate its contribution to the heat release also by a KJMA expression.

$$v_b = c_b^{max}\left(1-\exp\left\{(1-a(t-t_b)^{3/2})\right\}\right) \quad \text{for} \quad t \geq t_b \tag{6}$$

$$h_b(t) = h_b^{max}\left(1-\exp\left\{(1-a(t-t_b)^{3/2})\right\}\right) \quad \text{for} \quad t \geq t_b \tag{7}$$

A least-squares fit of $h_a + h_b$ to the DSC data shown in figure 5 as a solid line. A statistical analysis reveals the parameter values $h_a^{max} = 17.7$ J/g , $h_b^{max} = 2.0$ J/g, $A_0 = 0.35$, $t_b = 96$ min, $vt_b/r_0 = 0.67$ where the 95 % confidence intervals are in the range of 10 % to 20 % of the expectation values. It is obvious that the introduction of diffusion controlled mechanism

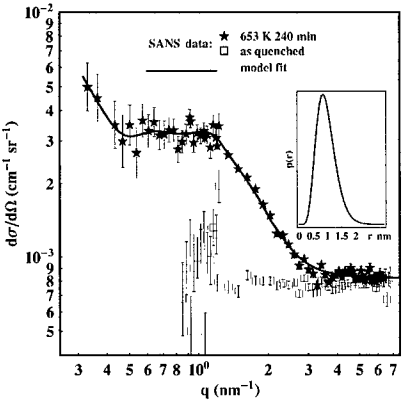

Figure 6: Sans data obtained from the as-prepared state and the annealed sample (240 min at 653 K). The solid line is a theoretical curve obtained with a model of polydisperse spherical particles with diffusion zones. The embedded picture shows the fitted probability density $p(r)$ of the particle sizes.

at a time t_b can explain both the results of the DSC experiment and the results from the SANS experiment. The question of physical background of this process arises naturally. We assume

that large locally ordered clusters become unstable during the growth. This assumption is suggested by theoretical and experimental results on the stability of clusters of atoms. It has been shown that icosahedral arrangement of atoms is energetically advantageous for small clusters consisting of several hundreds of atoms whereas for larger particles crystalline order is more favorable (see e.g. [33]). It is reasonable to assume the existence of icosahedral local packing in the present metallic glass since in similar alloys such as $Zr_{65}Cu_{17.5}Ni_{10}Al_{7.5}$ the formation of icosahedral phases was observed experimentally [34, 35]. Additionally at this stage of the process the packing fraction is so high that due to diffusion processes at the impinging surfaces the transformation into the crystalline state can be promoted. The change of the local chemical composition or their local boundary conditions can than lead to the scattering contrast increase observed by SANS. The onset of diffusion and/or the formation of nanocrystallites should be visible in the behavior of the shear viscosity γ of a sample subjected to isothermal annealing. Figure 7 shows the result of the corresponding

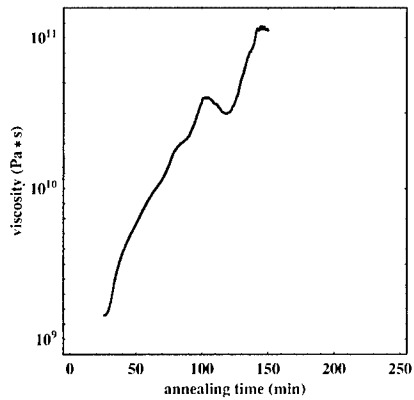

Figure 7: Evolution of the shear viscosity versus annealing time.

experiment carried at a constant uniaxial load using a Perkin-Elmer DSC 7E. There is a continuous increase of γ from the beginning of the thermal treatment at 653 K up to about 90 min. This increase can be understood as a decrease of the mean free $\bar{v_f}$ volume according to the expression

$$\gamma(t) \propto \exp\left\{\frac{v_c}{\bar{v_f}}\right\} \quad \text{with } v_c \text{ a critical value of } \bar{v_f} \tag{8}$$

In the interval from 100 min to 130 min annealing time the curve shows a significant dip indicating a temporarily increase of the mean free volume according to equation 8. So that also the shear viscosity recorded a significant change of its behavior at the same stage as SANS and DSC do. In this model the improvement of the medium-range order during annealing in the samples at constant properties of the next-nearest neighbor shell can be understood as the increase of the correlation length of local icosahedral packing realized by re-arranging

of small icosahedral structure units at the cluster surface. This also may explain a decrease of the free volume and a increase of the shear viscosity according to equation 8. The evolution of the correlation length r_{xrd} measured by XRD (see [13]) and its mean value of about 1.6 nm confirms this interpretation as well. We assume further on, that large noncrystalline clusters become unstable during their growth. Then the change of the chemical composition and/or their local boundary conditions lead to an transformation into the crystalline state. As mentioned above icosahedral arrangements of atoms are energetically advantageous for small clusters whereas for larger particles crystalline order is more favorable (see e.g. [33]). The volume fraction of locally ordered clusters at that stage of about 70 % leads to impinging of domains. An percolation threshold on the interconnected domain boundaries may occur and enhanced diffusion becomes possible. The SANS results were obtained under the assumption of a diffusion zone around spherical particles and a good evidences for its existence was found. All parameters obtained with the non-linear least-square fit are in a very good agreement with the results from HREM, DSC and XDR analysis. The methods together permit us to suggest a model with is in agreement with the data and theoretical considerations. Therewith this model is a contribution to explain the formation process of nanoscale structures in metallic glasses.

References

[1] W. Klement, R. H. Willens, and P. Duwez, Nature **187**, 869 (1960).

[2] Y. Yoshizawa, J. Metastable Nanocryst. Mater. **1**, 51 (1999).

[3] F. Sommer, Z. Metallk. **73**, 72 (1982).

[4] E. Nold, G. Rainer-Harbach, P. Lamparter, and S. Steeb, Z. Naturforsch. **38**, 325 (1984).

[5] E. Nassif, P. Lamparter, and S. Steeb, J. Non-Cryst. Solids **61-62**, 319 (1984).

[6] F. E. Fujita, in *in Rapidly Quenched Metals* (North-Holland, Amsterdam, 1985).

[7] M. Calin and U. Köster, Mater. Sci. Forum **269-272**, 749 (1998).

[8] U. Köster, A. Rüdiger, and J. Meinhardt, J. Metastable Nanocryst. Mater. **1**, 9 (1999).

[9] S. Schneider, P. Thiyagarajan, U. Geyer, and W. L. Johnson, Physica B **241-243**, 918 (1998).

[10] J. F. Löffler and W. L. Johnson, Appl. Phys. Lett. **76**, 3394 (2000).

[11] K. F. Kelton, Phil. Mag. Lett **77**, 337 (1998).

[12] H. Hermann, A. Heinemann, N. Mattern, and A. Wiedenmann, Euro. Phys. Lett. **51**, 127 (2000).

[13] N. Mattern, U. Kühn, J. Neuefeind, and J. Eckert, Appl. Phys. Lett. **77**, 1153 (2000).

[14] C. Fan and A. Inoue, Appl. Phys. Lett. **77**, 46 (2000).

[15] C. Fan and A. Inoue, Mater. Transactions *JIM* **40**, 1376 (2000).

[16] C. Fan and A. Inoue, C. Fan and C. Li and A. Inoue and V. Haas **61**, 3761 (2000).

[17] J. G. Wang, B. W. Choi, T. G. Nieh, and C. T. Liu, J. Mater. Res. **15**, 798 (2000).

[18] G. Porod, *Small Angle X-ray Scattering* (Academic Press, London, 1982).

[19] A. Heinemann, H. Hermann, A. Wiedenman, N. Mattern, and K. Wetzig, J. Appl. Cryst. **33**, 1386 (2000).

[20] N. W. Ashcroft and J. Lekner, Phys. Rev. **145**, 83 (1966).

[21] W. K. Bertram, J. Appl. Cryst. **29**, 682 (1996).

[22] H. Hermann, A. Heinemann, H.-D. Bauer, N. Mattern, U. Kühn, and A. Wiedenmann, J. Appl. Cryst. **34**, 666 (2001).

[23] A. Heuer, M. Wilhelm, H. Zimmermann, and H. W. Spiess, Phys. Rev. Lett. **75**, 2851 (1995).

[24] R. Böhmer, G. Hinze, G. Diezemann, B. Geil, and H. Sillescu, Europhys. Lett. **36**, 55 (1996).

[25] R. Zorn, Rev. B **5**, 6249 (1997).

[26] W. Kob, C. Donati, S. J. Plimpton, P. H. Poole, and S. C. Glotzer, Phys. Rev. Lett. **79**, 2827 (1997).

[27] C. Donati, J. F. Douglas, W. Kob, S. J. Plimpton, P. H. Poole, and S. C. Glotzer, Phys. Rev. Lett. **80**, 2338 (1998).

[28] D. Caprion and H. R. Schober, Phys. Rev. Lett. **85**, 4293 (2000).

[29] C. Kaur and S. P. Das, Phys. Rev. Lett. **86**, 2062 (2001).

[30] A. N. Kolmogorov, Izv. Akad. Nauk USSR. **2**, 355 (1937).

[31] W. A. Johnson and R. Mehl. Trans. AIME **135**, 416 (1939).

[32] M. Avrami, J. Chem. Phys. **7**, 1103 (1939).

[33] D. Holland-Moritz, J. Non-Equilibrium Processing **11**, 169 (1998).

[34] U. Köster, J. Meinhardt, S. Roos, and H. Liebertz, Appl. Phys. Lett. **169**, 179 (1996).

[35] J. Eckert, N. Mattern, M. Zinkevitch, and M. Seidel, Mater. Trans. JIM **39**, 623 (1996).